AIAA JOURNAL
Vol. 42, No. 6, June 2004

Reduced-Order Model Development Using Proper Orthogonal Decomposition and Volterra Theory

David J. Lucia* and Philip S. Beran†
U.S. Air Force Research Laboratory, Wright–Patterson Air Force Base, Ohio 45433-7531

A new approach for generating reduced-order models of fluid systems was developed using proper orthogonal decomposition in combination with Volterra theory. The method involves identifying fluid basis functions with proper orthogonal decomposition and applying systems realization theory to generate a low-dimensional model for the scalar coefficients. The method was tested on a two-dimensional inviscid flow over a bump with forcing. Eight fluid basis functions were identified, and the eigensystem realization algorithm was used to identify an eight-state, reduced-order model. Time histories of both the reduced-order coefficients and the expanded flowfield data accurately tracked the full-order results in both amplitude and phase (average error less than 5%). The reduced-order model demonstrated four-orders-of-magnitude reduction in compute time relative to the full system, which represents a computational improvement on the same order as the reduction in degrees of freedom.

Nomenclature

A, B, C	=	state-space matrix operators
$a(t)$	=	modal coefficient
D, P, Q	=	singular value decomposition products
$\boldsymbol{E}, \boldsymbol{F}$	=	vector of X-axis and Y-axis fluxes
E_T	=	total energy, $E_{Td}/\rho_\infty u_\infty^2$
f_{mod}	=	modulating spatial function
$g(t)$	=	modulating time function
H_{rs}	=	generalized Hankel matrix
$\boldsymbol{h}$	=	volterra kernel function
$\hat{\boldsymbol{\imath}}$	=	unit vector, x direction
$\hat{\boldsymbol{\jmath}}$	=	unit vector, y direction
K	=	number of time samples in impulse
k	=	index on summation
L	=	reference length
M	=	number of degrees of freedom (DOFs) for proper orthogonal decomposition/reduced-order modeling (POD/ROM)
m_x, m_y	=	fluid momentum components, ρu, ρv
N	=	number of DOFs for full system
n	=	time index
P	=	pressure, $P_d/\rho_\infty u_\infty^2$
Q	=	number of snapshots used in POD/ROM
q	=	number of states in realization
R	=	flux calculation from the Euler equations
r	=	size of shift in data window
S	=	matrix of flow field data, or snapshots
s	=	number of time samples in window
t	=	time, $t_d u_\infty/L$
U	=	continuous conserved flow variables
$\boldsymbol{U}, \hat{\boldsymbol{U}}$	=	full- and reduced-order vector of discrete conserved flow variables
$\boldsymbol{u}$	=	vector of forcing inputs
u, v	=	fluid velocity components, u_d/u_∞, v_d/u_∞
V	=	matrix of eigenvectors of $S^T S$
$\boldsymbol{w}, \hat{\boldsymbol{w}}$	=	full- or reduced-order vector for a single fluid variable
$\boldsymbol{X}$	=	spatial position vector, (x, y)
$\boldsymbol{x}$	=	vector of dynamic states
x, y	=	spatial coordinates, x_d/L, y_d/L
$\boldsymbol{Y}$	=	Markov parameter
$\boldsymbol{y}$	=	vector of measurement data
α	=	forcing amplitude
β	=	scaling parameter
γ	=	ratio of specific heats
Δt	=	time-step size for integration
ρ	=	density, ρ_d/ρ_∞
Φ	=	reduced-order mapping matrix
$\phi(\boldsymbol{X})$	=	POD basis function
$\boldsymbol{\phi}$	=	POD basis vector
ω	=	forcing frequency

Subscripts

d	=	dimensional quantity
f	=	fluid system
n	=	Volterra kernel index
0	=	base flow
∞	=	freestream quantity, dimensional

Introduction

THIS research merges two of the more prevalent reduced-order modeling (ROM) techniques currently being developed for nonlinear compressible flows: Volterra methods and proper orthogonal decomposition (POD). The application of ROM techniques to compressible flows is an active area of research, motivated by the desire for faster flow solvers that are well suited to the design environment. For example, transonic, fluid–structure interaction is a particular application of interest to both external and internal aerodynamicists because moving shock waves in a flow necessitate high-fidelity numerical flow solvers, which are too cumbersome for iterative design analysis. Regardless of the application, when nonlinearities are present in the flowfield established order-reduction methods that rely on linearized dynamics are of little use.

POD of flow simulations was introduced in the mid-1990s to reduce the number of degrees of freedom (DOFs) of flow solvers. The literature refers to such POD based fluid models as POD reduced-order models (ROMs), where the term *order* is used to imply the number of DOF. POD essentially identifies a small number of global

Received 30 October 2002; revision received 16 May 2003; accepted for publication 30 December 2003.

*Major, USAF, AFRL/VASD, Building 146, 2210 Eighth Street; david.lucia@wpafb.af.mil. Member AIAA.

†Principal Research Aerospace Engineer, AFRL/VASD, Building 146, 2210 Eighth Street; philip.beran@wpafb.af.mil. Associate Fellow AIAA.

fluid modes. A variety of techniques are used to identify the time-varying modal coefficients. POD/ROM has enjoyed a great deal of success for incompressible flowfields. Computers using the POD reduced-order models can produce data fast enough to enable some types of flow control for incompressible flows (e.g., see Refs. 1–6). Galerkin projection was used in conjunction with POD to yield these results.

More recently, POD has been extended to compressible flow applications, but difficulties in solving for the modal amplitudes have limited computational performance. POD/ROMs using non-Galerkin solvers have been successfully applied to subsonic flow, and supersonic aeroelastic problems for the case when the shock motion and/or oscillations of any separated flow region are linearly proportional to the structural motion. Such models are sufficient to predict the onset of flutter and also limit-cycle oscillations if the dominant nonlinearity is structural rather than aerodynamic in origin. Of course if an aerodynamic nonlinearity caused by large shock motions or large oscillations of a separated flow region is the principal cause of the limit-cycle oscillations, then assuming that such motions are linearly proportional to the structural motion is not sufficient.[7–15] POD has also been used for low-speed airfoil design.[16] Recent advances in reduced-order modeling for internal flows have considered small motions of a transonic shock in turbomachinery.[17–20] Using domain decomposition, POD/ROM has also been successfully applied to flows with large motions of strong shocks.[21,22] The extension of POD/ROM to compressible flow has produced as much as three-orders-of-magnitude reduction in DOFs, but the best, nonlinear solvers have only realized one order of magnitude in computational savings.[22–24] If the order reduction represents the potential in computational savings from using POD/ROM, current nonlinear implementations are not efficiently exploiting the low-order behavior.

Another ROM approach using Volterra series has been successfully applied to nonlinear aeroelastic systems.[25] Volterra methods rely on an inverse approach, where the dynamics of a physical system are synthesized from a systematic collection of responses to known inputs. The Volterra series consists of integral operators that modify the system input using Volterra kernels. The sum of the series produces the system response. For linear, time-invariant systems the Volterra series is the convolution integral, and the Volterra kernel is the system impulse response. The higher-order Volterra kernels vanish for linear systems, but nonlinear systems require additional terms. Both linear and nonlinear Volterra kernels can be readily identified from empirical data using both frequency-domain and time-domain techniques[26–29]; however, integration of the higher-order terms in the series is computationally demanding. Researchers in this area are currently looking for ways to employ systems realization theory to produce linearized and nonlinear state-space systems that can be easily integrated. For first-order Volterra kernels, the eigensystem realization algorithm (ERA) has been identified as a viable systems-realization technique.[30] One drawback of the Volterra approach is that it provides scalar outputs to scalar inputs. Application of Volterra methods to a spatially distributed flowfield implies a large scalar system because every location of interest would represent four states in two dimensions within the convolution integral (one state per fluid variable, five in three dimensions). The Volterra approach is not efficient for such large systems.

This paper extends the application of Volterra theory to reduced-order modeling of compressible flows by considering the modal response of global fluid modes obtained through proper orthogonal decomposition. Volterra theory has been used with good success on structural dynamics applications.[30] Even though structural systems are spatially distributed, the number of states is reduced through modal analysis. The Volterra approach is applied to scalar modal amplitudes, which provides a small set of time signals for systems realization. Proper orthogonal decomposition provides an analogous approach for fluid flows. Global fluid modes are identified with POD, and systems realization theory is used to identify the modal responses from numerical data. The numerical data are the response of the fluid flow to the impulse excitation of one or more forcing terms. The fluid response at each sampled time is projected onto the POD basis functions to obtain the time history of the modal amplitudes. The resulting data are used to synthesize a very low-order state-space model, which can be integrated quickly to obtain time histories of the modal amplitudes. The entire flowfield can be reconstructed from the modal amplitudes for any time of interest.

The hybrid POD-Volterra approach is demonstrated using a linear flowfield undergoing oscillatory forcing within the interior of the domain. Following a more detailed discussion of POD, Volterra theory, and ERA, a systematic procedure is developed to synthesize a linear state-space model using the POD basis functions. Details of the approach are provided, concentrating on discrete-time impulse response generation using the full-order model and system identification using ERA. The accuracy of the state-space model is addressed by expanding the reduced-order time history to obtain unsteady flowfield data, which are then compared with the full-order results. For comparison, the nonlinear, non-Galerkin approach to POD/ROM is also applied to this problem, and the computational performance of the hybrid approach is shown to be vastly superior. Lastly, the potential for nonlinear analysis using the POD-Volterra approach is discussed.

For time linearized models where the shock motion is assumed linearly proportional to the structural motion, POD/ROM is a highly efficient solution method shown to reduce computational cost by several orders of magnitude. This method also works for transonic viscous flows if any separated flow regime undergoes oscillations whose amplitude is linearly proportional to the structural motion. For large motions of the shock or separated flow such that these motions are no longer linearly proportional to the structural motion, extending POD/ROM is straightforward in principle but very difficult in practice because of the particular form in which computational-fluid-dynamics (CFD) codes and their equations are usually structured as discussed in this paper. However, the harmonic balance technique, which solves for nonlinear unsteady periodic flows by expanding the solution in a Fourier series of harmonics in time, has been shown to reduce the cost of CFD solutions relative to a time-marching method.[17] The method discussed in the present paper, when extended to the case of large shock motions and large oscillations of separated flows, seeks to further reduce this computational time.

Background

Fluid Dynamics

The dynamics of inviscid fluid flows are governed by the Euler equations. The two-dimensional Euler equations are given next in strong conservation form[31]:

$$\frac{\partial U}{\partial t} + \frac{\partial E}{\partial x} + \frac{\partial F}{\partial y} = 0 \tag{1a}$$

$$U(\boldsymbol{X}, t) = \begin{bmatrix} \rho \\ m_x \\ m_y \\ E_T \end{bmatrix} \tag{1b}$$

$$E = \begin{bmatrix} m_x \\ -\dfrac{m_x^2(\gamma-3) + (\gamma-1)\left(m_y^2 - 2E_T\rho\right)}{2\rho} \\ \dfrac{m_x m_y}{\rho} \\ \dfrac{m_x\left[m_x^2(1-\gamma) - m_y^2(\gamma-1) + 2E_T(1+\gamma)\rho\right]}{2\rho^2} \end{bmatrix}$$

$$F = \begin{bmatrix} m_x \\ \dfrac{m_x m_y}{\rho} \\ -\dfrac{m_y^2(\gamma-3) + m_x^2(\gamma-1) - 2E_T(\gamma-1)\rho}{2\rho} \\ \dfrac{m_y\left[m_x^2(1-\gamma) - m_y^2(\gamma-1) + 2E_T\gamma\rho\right]}{2\rho^2} \end{bmatrix}$$

where ρ, m_x, m_y, and E_T are functions of space and time. Because we assume an ideal gas for our applications, this equation set can be closed using the ideal-gas law.

The solution of the Euler equations can be approximated using either finite difference, finite volume, or finite element techniques. To do this, the spatial domain is discretized, and the flow variables in $U(\boldsymbol{X}, t)$ at each discrete location are collocated into a column vector $\boldsymbol{U}(t)$. Time integration across the computational mesh is used to obtain flow solutions.

Because the Euler equations are linear in the time derivative, and quasi-linear in the spatial derivative,[31,32] the spatial derivatives and the time derivatives in Eq. (1a) can be separated to form an evolutionary system. To accomplish this, the spatial derivatives of the flux terms $\partial E/\partial x$ and $\partial F/\partial y$ are grouped to form a nonlinear operator R acting on the set of fluid variables. The fluid dynamics from Eq. (1a) can then be expressed as

$$\frac{\mathrm{d}U(\boldsymbol{X}, t)}{\mathrm{d}t} = R[U(\boldsymbol{X}, t)] \tag{2}$$

When discretized, this expression takes the form

$$\frac{\mathrm{d}\boldsymbol{U}(t)}{\mathrm{d}t} = R[\boldsymbol{U}(t)] \tag{3}$$

Equation (3) is referred to as the full-system dynamics.

Proper Orthogonal Decomposition

POD is a technique to identify a small number of basis functions that adequately describe the behavior of the full-system dynamics [Eq. (3)] across some parameter space of interest. A summary of POD as it applies to a spatially discretized flowfield follows. A detailed description of POD is available in the literature.[23,33] For simplicity, consider only one fluid variable $w(\boldsymbol{x}, t)$, which when spatially descritized using N nodes is denoted $\boldsymbol{w}(t)$. For this fluid variable, the full-system dynamics in Eq. (3) is expressed as

$$\frac{\mathrm{d}\boldsymbol{w}}{\mathrm{d}t} = R_w(\boldsymbol{w}) \tag{4}$$

Spectral methods approximate the solution $w(\boldsymbol{X}, t)$ as

$$w(\boldsymbol{X}, t) \approx \sum_{k=1}^{M} a_k(t)\phi_k(\boldsymbol{X}) \tag{5}$$

When the domain is spatially discretized, $\phi_k(\boldsymbol{X})$ becomes a vector ϕ_k, and the following relation applies:

$$\boldsymbol{w}(t) \approx \sum_{k=1}^{M} a_k(t)\phi_k \tag{6}$$

The set of vectors $\{\phi_k\}$ are discrete basis functions corresponding to the computational mesh defined for the numerical solver. The set $\{a_k\}$ are the modal coefficients, and Eq. (6) can be represented using matrix algebra. The fluid modes comprise columns of a modal matrix Φ, and the coefficients are collocated into a column vector $\hat{\boldsymbol{w}}(t)$. POD produces a linear transformation Φ between the full-order solution $\boldsymbol{w}$ and the reduced-order solution $\hat{\boldsymbol{w}}$:

$$\boldsymbol{w}(t) = \boldsymbol{W}_0 + \Phi\hat{\boldsymbol{w}}(t) \tag{7}$$

The reduced-order variable $\hat{\boldsymbol{w}}(t)$ represents deviations of $\boldsymbol{w}(t)$ from a base solution $\boldsymbol{W}_0$. The subtraction of $\boldsymbol{W}_0$ will result in zero-valued boundaries for the POD modes wherever constant boundary conditions occur on the domain.

Φ is constructed by collecting observations of the solution $\boldsymbol{w}(t) - \boldsymbol{W}_0$ at different time intervals throughout the time integration of the full-system dynamics. These observations are called snapshots[34] and are generally collected to provide a good variety of flowfield dynamics while minimizing linear dependence. The snapshot generation procedure is sometimes referred to as POD training.[23]

A total of Q snapshots are collected from the full-system dynamics. These are vectors of length N. The set of snapshots describe a linear space that is used to approximate both the domain and the range of the nonlinear operator R_w. The linear space is defined by the span of the snapshots.[35] POD identifies a new basis for this linear space that is optimally convergent[33] in the sense that no other set of basis functions will capture as much energy in as few dimensions as the POD basis functions. To identify the POD basis, the snapshots are compiled into an $N \times Q$ matrix S, known as the snapshot matrix. The mapping function Φ is then developed using

$$S^T S V = V\Lambda \tag{8a}$$

$$\Phi = SV \tag{8b}$$

Here V is the matrix of eigenvectors of $S^T S$, and Λ is the corresponding diagonal matrix of eigenvalues. To eliminate redundancy in the snapshots, the columns of V corresponding to very small eigenvalues in Λ are truncated. The matrix of eigenvalues Λ is also resized to eliminate the rows and columns corresponding to the removed eigenvalues. If $Q - M$ columns of V are truncated, the resulting reduced-order mapping Φ will be an $N \times M$ matrix. Φ determines the coordinates of $\boldsymbol{w}(t)$ in terms of the M remaining basis functions ϕ_k.

The reduced-order mappings for each fluid variable are developed separately, and individual S and V arrays are collocated as blocks into a larger set of arrays, also denoted S and V, to form

$$\boldsymbol{U}(t) \approx \boldsymbol{U}_0 + \Phi\hat{\boldsymbol{U}}(t) \tag{9a}$$

$$\Phi = SV \tag{9b}$$

These versions of Eqs. (7) and (8b), respectively, apply to the entire set of fluid variables.

Reduced-Order Model Generation

Once the POD basis functions have been identified using the method of snapshots, the Euler equations must be recast to solve for the modal coefficients $\hat{\boldsymbol{U}}(t)$ in lieu of the full-system variables $\boldsymbol{U}(t)$. For compressible flows, this is generally accomplished using a non-Galerkin method.

The non-Galerkin approach, also known as the subspace projection method,[9] uses the full-system dynamics and a forward difference approximation to yield the following reduced-order flow solver:

$$\hat{\boldsymbol{U}}^{n+1} = \hat{\boldsymbol{U}}^n + \Delta t\,\Lambda^{-1}(V^T V)^{-1} V^T S^T R(SV\hat{\boldsymbol{U}}^n) \tag{10}$$

The pseudoinverse of V is shown assuming modal truncation is employed. The inverse of Λ and pseudoinverse of V exist assuming modal truncation is employed to eliminate the zero-valued eigenvalues of $S^T S$ and their corresponding eigenvectors.[36] Notice that $\Lambda^{-1}(V^T V)^{-1} V^T S^T$ from Eq. (10) is equivalent to $(\Phi^T\Phi)^{-1}\Phi^T$, and $(\Phi^T\Phi)^{-1}\Phi^T = \Phi^T$ when the modes are normalized.

The subspace projection method relies on the full-system function evaluation R at each time-integration step. As such, the order of each integration step is not actually reduced. Computational improvement occurs because subspace projection can greatly increase the time-step size allowed for stability. The total number of time

steps required for the explicit solver can be significantly reduced using this approach.[23]

Volterra Methods

This section will concentrate on time-domain Volterra formulations,[37–39] consistent with the implied application to time-domain, computational-fluid-dynamics methods. The literature on Volterra theory is rich, including several texts.[26,40–42]

First consider time-invariant, nonlinear, continuous-time systems. Of interest is the response of the system about an initial state $\boldsymbol{x}(0) = \boldsymbol{x}_0$ as a result of an arbitrary input $u(t)$ (we take u as a real, scalar input) for $t \geq 0$. As applied to these systems, Volterra theory yields the response

$$\boldsymbol{x}(t) = \boldsymbol{h}_0 + \int_0^t \boldsymbol{h}_1(t-\tau)u(\tau)\,\mathrm{d}\tau + \int_0^t \int_0^t \boldsymbol{h}_2(t-\tau_1, t-\tau_2)u(\tau_1)u(\tau_2)\,\mathrm{d}\tau_1\,\mathrm{d}\tau_2 + \sum_{n=3}^{N} \int_0^t \cdots \int_0^t \boldsymbol{h}_n(t-\tau_1, \ldots, t-\tau_n)u(\tau_1)\ldots u(\tau_n)\,\mathrm{d}\tau_1 \ldots \mathrm{d}\tau_n \tag{11}$$

The Volterra series in expression (11) contains three classes of terms. The first is the steady-state term satisfying the initial condition $\boldsymbol{h}_0 = \boldsymbol{x}_0$. Next is the first response term,

$$\int_0^\infty \boldsymbol{h}_1(t-\tau)u(\tau)\,\mathrm{d}\tau$$

where $\boldsymbol{h}$ is known as the first-order kernel (or the linear unit impulse response). The identification of the kernel $\boldsymbol{h}(\tau_1)$ is based on measuring the response of the system to a unit impulse (Dirac delta function) at $\tau_1 = 0$. Equation (11) requires the system to be time invariant, so that the system responds in an identical manner (but translated in time) to an impulse at any $\tau_1 > 0$. The first response term represents the convolution of the first-order kernel with the system inputs for times between 0 and t, where by causality inputs beyond time t are excluded. Last are the higher-order terms involving the second-order kernel $\boldsymbol{h}_2$ and the nth-order kernels $\boldsymbol{h}_n$. These terms do not all vanish when the system is nonlinear.[38]

The Volterra series can be accurately truncated beyond the second-order term when a weakly nonlinear formulation is considered:

$$\boldsymbol{x}(t) = \boldsymbol{h}_0 + \int_0^t \boldsymbol{h}_1(t-\tau)u(\tau)\,\mathrm{d}\tau + \int_0^t \int_0^t \boldsymbol{h}_2(t-\tau_1, t-\tau_2)u(\tau_1)u(\tau_2)\,\mathrm{d}\tau_1\,\mathrm{d}\tau_2 \tag{12}$$

The assumption of a weakly nonlinear system is consistent with the emergence of limit-cycle oscillation of a two-dimensional aeroelastic system in transonic flow through a supercritical Hopf bifurcation.[9] For linear systems, only the first-order kernel is nontrivial, and there are no limitations on input amplitude.

The first- and second-order kernels are presented next in final form[37]:

$$\boldsymbol{h}_1(\tau_1) = 2\boldsymbol{x}_0(\tau_1) - \tfrac{1}{2}\boldsymbol{x}_2(\tau_1) \tag{13}$$

$$\boldsymbol{h}_2(\tau_1, \tau_2) = \tfrac{1}{2}[\boldsymbol{x}_1(\tau_1, \tau_2) - \boldsymbol{x}_0(\tau_1) - \boldsymbol{x}_0(\tau_2)] \tag{14}$$

In Eq. (13), $\boldsymbol{x}_0(\tau_1)$ is the time response of the system to a unit impulse applied at time 0, and $\boldsymbol{x}_2(\tau_1)$ is the time response of the system to an impulse of twice unit magnitude at time 0. These response functions represent the memory of the system. If the system is linear, then $\boldsymbol{x}_2 = 2\boldsymbol{x}_0$ and $\boldsymbol{h}_1 = \boldsymbol{x}_0$, which is why the first-order kernel is referred to as the linear unit impulse response. The identification of the second-order kernel is more demanding because it is dependent on two parameters. Assuming $\tau_2 > \tau_1$ in Eq. (14), $\boldsymbol{x}_0(\tau_2)$ is the response of the system to an impulse at time τ_2.

Time is discretized with a set of time steps of equivalent size. Time levels are indexed from 0 (time 0) to n (time t), and the evaluation of $\boldsymbol{x}$ at time level n is denoted by $\boldsymbol{x}[n]$. The convolution in discrete time is

$$\boldsymbol{x}[n] = \boldsymbol{h}_0 + \sum_{k=0}^{N} \boldsymbol{h}_1[n-k]u[k] \tag{15}$$

$$+ \sum_{k_1=0}^{N} \sum_{k_2=0}^{N} \boldsymbol{h}_2[n-k_1, n-k_2]u[k_1]u[k_2] \tag{16}$$

The identification of linearized and nonlinear Volterra kernels is an essential step in the development of ROMs based on Volterra theory, but it is not the final step. Ultimately, these functional kernels can be transformed into linearized and nonlinear (bilinear) state-space systems that can be easily implemented into other disciplines such as controls and optimization.[26,37] For linear dynamics, state-space realization using the ERA has been used to generate linear, aeroelastic systems.[30] Nonlinear system realization is an active area of research.

System Realization

The ERA method[43] identifies a discrete, linear, time-invariant state-space realization of the form

$$\boldsymbol{x}[n+1] = A\boldsymbol{x}[n] + B\boldsymbol{u}[n], \qquad \boldsymbol{y}[n] = C\boldsymbol{x}[n] \tag{17}$$

using data from a complete ensemble of impulse responses. Initial state responses can be used in lieu of impulse responses, but we only consider impulse response data in this overview for simplicity. The systems realization procedure takes measurement data $\boldsymbol{y}[n]$ from the free response of the system and produces a minimal state-space model A, B, and C such that functions $\boldsymbol{y}$ are accurately reproduced.

The free pulse response of linear, time-invariant, discrete systems is given by a function known as the Markov parameter:

$$\boldsymbol{Y}[n] = CA^{n-1}B \tag{18}$$

The superposition principle states that a system response to any arbitrary input can be obtained from a linear combination of impulse responses from that system. The generalized Hankel matrix of impulse responses is related to the Markov parameter by the superposition principle. The Hankel matrix is formed by windowing the impulse response data. A total of K data points are provided at discrete time steps $t = t_1, \ldots, t_K$, and the $r \times s$ matrix H_{rs} is formed as follows:

$$H_{\mathrm{rs}}^{n-1} = \begin{bmatrix} \boldsymbol{Y}[n] & \cdots & \boldsymbol{Y}[n+t_{s-1}] \\ \boldsymbol{Y}[j_1+n] & \cdots & \boldsymbol{Y}[j_1+n+t_{s-1}] \\ \vdots & \vdots & \vdots \\ \boldsymbol{Y}[j_{r-1}+n] & \cdots & \boldsymbol{Y}[j_{r-1}+n+t_{s-1}] \end{bmatrix} \tag{19}$$

The choice of r and s is arbitrary as long as $r + s + k \leq K + 2$.

The ERA method eliminates redundant data by using singular value decomposition (SVD) on H_{rs}^0,

$$H_{\mathrm{rs}}^0 = PDQ^T \tag{20}$$

Unwanted state dimensionality is eliminated by truncating the elements of P, D and Q associated with very small singular values of H_{rs}^0. The number of states is reduced to a minimal number q. The number of observations p and the number of forcing terms m are known from the problem formulation. The dimension of the Markov parameter $\boldsymbol{Y}[n]$ is $p \times m$. Algebra is used to recast Eq. (18) in terms of the time-shifted Hankel matrix $\boldsymbol{H}_{\mathrm{rs}}^1$ and the elements P, D, and

Q. The state-space realization flows from this manipulation and is as follows:

$$A = D^{-\frac{1}{2}} P^T H_{\text{rs}}^1 Q D^{-\frac{1}{2}} \tag{21a}$$

$$B = D^{\frac{1}{2}} Q^T E_m \tag{21b}$$

$$C = E_p^T P D^{\frac{1}{2}} \tag{21c}$$

E_p^T and E_m^T are defined here:

$$E_p^T = [I_p, 0_p, \ldots, 0_p] \tag{22a}$$

$$E_m^T = [I_m, 0_m, \ldots, 0_m] \tag{22b}$$

where 0_p and 0_m as the null matrices of order p and m, respectively, and I_p and I_m are the identity matrices of order p and m.

Two-Dimensional Flow over a Bump with Forcing

A full-order numerical solver was developed to provide data for the POD basis, as well as a reliable solution for comparison with the reduced-order model results. The full-order model is described next, along with the key features of the resulting flowfield that we used to assess the performance of the POD-Volterra method.

Problem Description

POD-Volterra ROM development was demonstrated for a two-dimensional, inviscid flow along a solid wall containing a small circular arc. Unsteadiness was introduced by varying γ according to

$$\gamma(\boldsymbol{X}, t) = \gamma_{xy}(\boldsymbol{X}) + g(t) f_{\text{mod}}(\boldsymbol{X}) \tag{23}$$

The function $\gamma_{xy}(\boldsymbol{X})$ was the base value of γ when no forcing was applied. We used a constant value of $\gamma_{xy}(\boldsymbol{X}) = 1.4$ for our research. $f_{\text{mod}}(\boldsymbol{X})$ was a two-dimensional Gaussian distribution as depicted graphically in Fig. 1. The circular arc (length 1 and height 0:001) was centered at $x = 0$, $y = 0$, and the Gaussian curve was centered directly above it at $x = 0$, $y = 2.5$. The covariance terms determine the spread of the Gaussian curve and were $\sigma_x = \sigma_y = 0.25$. The time-varying function $g(t)$ was defined as

$$g(t) = \alpha \sin[\omega(t + t_{\text{base}})] \tag{24}$$

The scalar t_{base} adjusted the phase of the forcing to match initial flow conditions for starting the time integration at times other than $t = 0$. For the results that follow, the amplitude was fixed at $\alpha = 0.07$, and frequency was fixed at $\omega = 0.2145$. This type of forcing was selected to provide unsteady behavior without the added complication of a dynamic boundary condition.

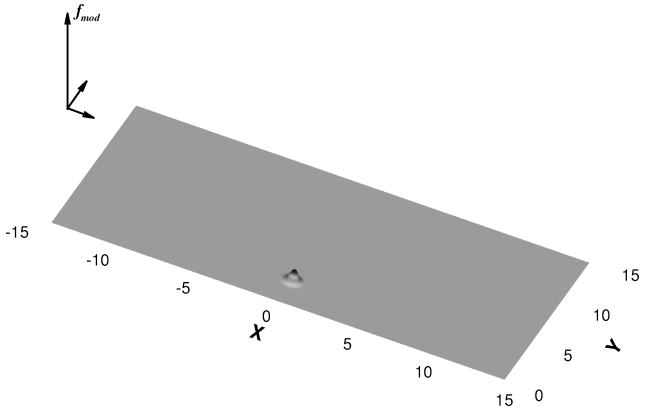

Fig. 1 Modulating function for γ.

Grid

A rectangular domain of dimension $-23.668 < x < 23.668$ and $0 < y < 24.6$ was used for this research. The large domain was intended to contain all of the flow dynamics, and extending the domain in this fashion facilitated the use of characteristic boundary conditions for the outer portion of the domain. A structured grid was generated for this domain using 141 nodes along the solid surface and 116 nodes extending to the far-field boundary. The spacing of the grid points increased geometrically from the solid wall in the normal direction. In the streamwise direction, the grid spacing was held constant at $\Delta_{\text{wall}} = 0.0125$ over the entire bump and was increased geometrically upstream and downstream of the bump position. This particular grid was shown to be converged for a similar inviscid flow problem using a comparable fluid solver.[44]

Solver

A finite volume scheme was the basis for the full-order solver used in this research, which approximated the integral form of the Euler equations:

$$\frac{\mathrm{d}}{\mathrm{d}t} \int_V U \, \mathrm{d}\mathcal{V} + \int_{\partial V} (E\hat{\boldsymbol{\imath}} + F\hat{\boldsymbol{\jmath}}) \cdot \mathrm{d}\bar{\mathcal{S}} = 0 \tag{25}$$

The grid points in the computational mesh described earlier were used to form corners for cells. For each cell, the integral form of

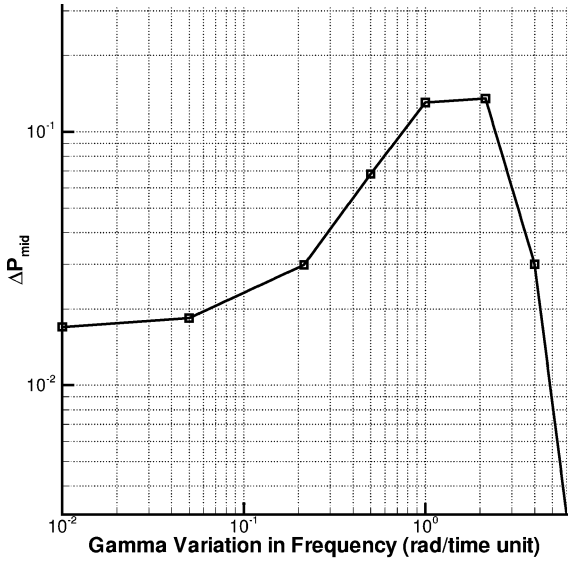

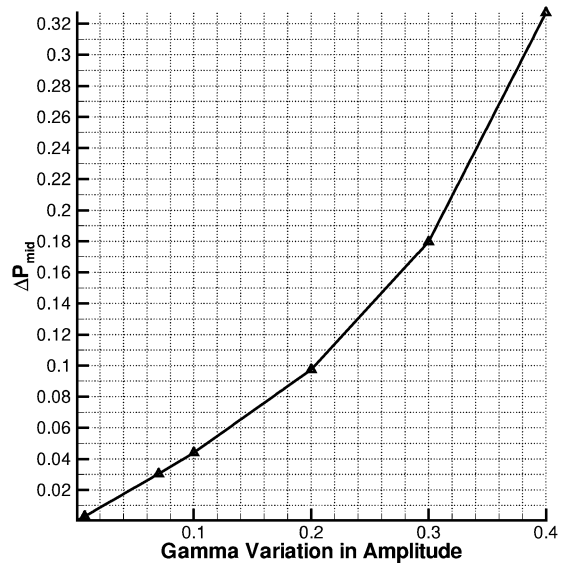

Fig. 2 Full-order pressure response.

the Euler equations reduced to the following, assuming no grid deformation:

$$\frac{\mathrm{d}}{\mathrm{d}t}U_{i,j} + \sum_{\text{sides}}(E_{i,j}\hat{\boldsymbol{\imath}} + F_{i,j}\hat{\boldsymbol{\jmath}}) \cdot \frac{\mathrm{d}\bar{\mathcal{S}}_{i,j}}{\mathrm{d}\mathcal{A}_{i,j}} = 0 \tag{26}$$

The flux terms $E_{i,j}$ and $F_{i,j}$ were computed using first-order Roe averaging,[31] and the flow variables $U_{i,j}$ were evaluated as cell averages. Time integration across the computational mesh was used to obtain flow solutions. This was accomplished with a first-order-accurate, forward Euler approximation. The full-order model for this problem had 64,400 DOFs.

External boundaries were handled with ghost cells. The fluid values for the ghost cells at the far-field boundaries were determined using characteristic boundary conditions.[31] The bump-surface was modelled using a transpiration approximation.[45] The finite volume fluid solver and the transpiration boundary condition were validated by comparison with experimental data.[46]

Full-Order Behavior

The full-order model was time integrated using the baseline forcing frequency $\omega = 0.2145$, the baseline amplitude variation of $\alpha = 0.07$, and a freestream Mach number $M_\infty = 0.75$. The flow was initialized with steady-state conditions obtained with zero forcing.

Once the flow was fully developed, the unsteady pressure on the surface of the bump varied based on the amplitude and frequency of the forcing term. The difference between the maximum and minimum surface pressures (nondimensional, for fully developed flow) at the half-chord location on the bump surface is denoted ΔP_{mid}. The response of ΔP_{mid} from the full system is shown in Fig. 2 for variations in both frequency and amplitude. At the baseline amplitude, forcing frequencies greater than 0.1 introduced nonlinearities into the dynamics as indicated by the resonance peak in Fig. 2. At forcing frequencies between 0.1 and 0.5, the nonlinearities were weak. The average midpoint pressure was 1.265, which was slightly less than the freestream pressure $P_\infty = 1/\gamma M^2 = 1.27$. This difference was 33% of the pressure amplitude variation and provided a measure of nonlinearity. At frequencies between 0.5 and 3, the nonlinearities were stronger, and at frequencies greater than 3 the fluid system did not react quickly enough for forcing to affect pressure on the bump surface, and the frequency response quickly fell off. At the baseline frequency, amplitude variation greater than 0.1 introduced nonlinearities as well. The $\alpha = 0.07$ baseline amplitude was well within the linear range at this frequency.

Results

The POD-Volterra method is used to identify a low-order, state-space system for the unsteady bump problem with freestream Mach 0.75 as just described. The time history of $\hat{\boldsymbol{U}}$ is compared with the time history from the full-order system at the baseline forcing frequency $\omega = 0.2145$ and forcing amplitude $\alpha = 0.07$ to quantify the accuracy and computational efficiency of the reduced-order method.

Identification of Fluid Modes

Fluid modes were obtained using POD as outlined previously. S contained snapshots from time integration of the full-order model at the baseline frequency and amplitude. A set of 50 snapshots was taken at even intervals from startup through a single cycle of oscillation (approximately 28 time units). The base flow term $\boldsymbol{U}_0$ from Eq. (9a) consisted of freestream conditions everywhere throughout the domain. The first two modes for each fluid variable contained over 99% of the energy content, and system realization was performed using a total of $M = 8$ fluid modes (two modes per fluid variable).

System Realization

A state-space realization of the form in Eq. (17) was obtained using ERA. Impulse responses for the fluid system were generated using a single time-step pulse of $g(t)$ within the gamma-modulating function [Eq. (23)]. The impulse amplitude was arbitrarily chosen to be 1000. The full-system response to this impulse was sampled over 15 nondimensional time units at a rate of $\mathrm{d}t = 0.0244$ for a total of $K = 614$ discrete data points. The fluid system impulse response was generated using the full-order model. The time history of the full-order impulse response was projected onto each of the POD basis functions to obtain the impulse response of the reduced-order fluid variable $\hat{\boldsymbol{U}}$. The data were windowed using $s = 305$ and $r = 20$. Because there was only one forcing term, the value of m was 1, and $p = 8$ was chosen to match the number of ROM coefficients. The collection of impulse responses formed an 8×1 Markov parameter $\boldsymbol{Y}[n]$ function from Eq. (18). The number of states $q = 8$ was chosen

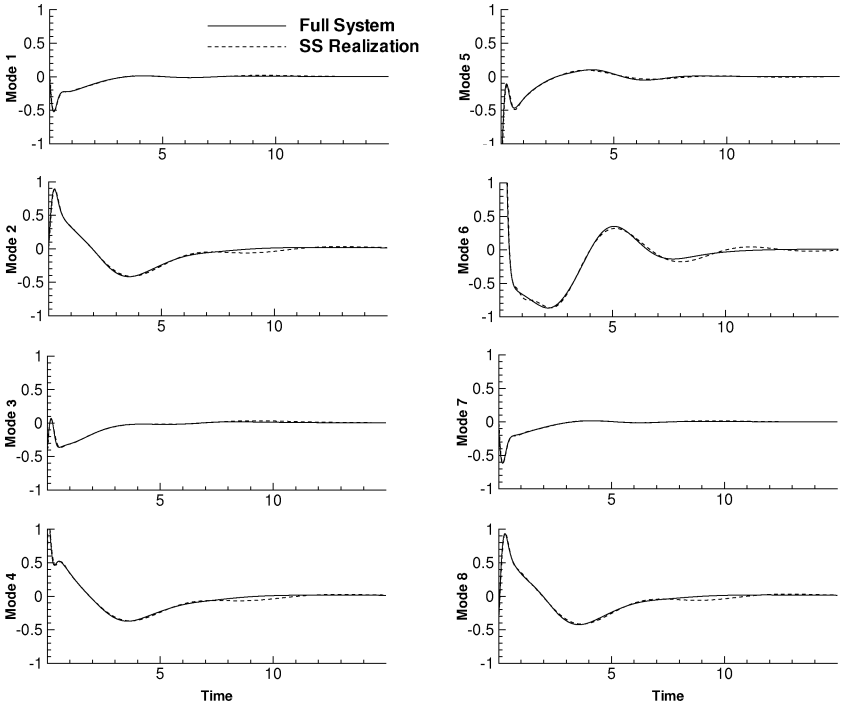

Fig. 3 Impulse response of state-space realization.

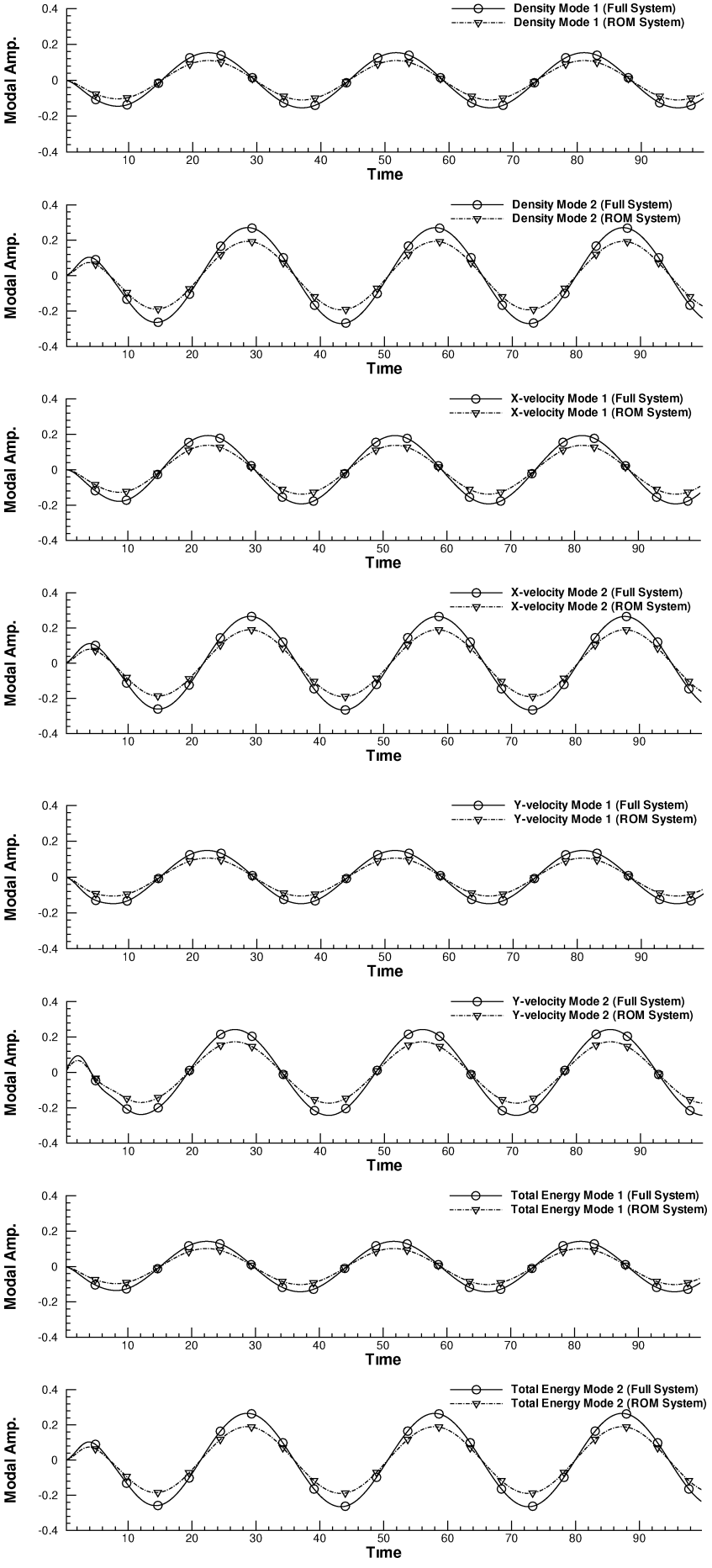

Fig. 4 Modal responses.

to match the number of ROM coefficients, so that SVD on the Hankel matrix formed from $\boldsymbol{Y}[n=1]$ was used to truncate all but the largest eight singular values, yielding the matrices P, D, and Q. Equations (21a–21c) were then used to generate a linear state-space model for the reduced-order fluid system:

$$\boldsymbol{x}[n+1] = A\boldsymbol{x}[n] + B\beta g[n] \tag{27a}$$

$$\hat{\boldsymbol{U}}[n] = C\boldsymbol{x}[n] \tag{27b}$$

where β is a scaling parameter that was used to calibrate the forcing amplitude. Because $\boldsymbol{x}$ and $\hat{\boldsymbol{U}}$ had the same dimensions, Eq. (27a) was simplified by dropping Eq. (27b),

$$\hat{\boldsymbol{U}}[n+1] = A_f\hat{\boldsymbol{U}}[n] + B_f\beta g[n] \tag{28}$$

where $A_f = CAC^{-1}$, $B_f = CB$, and $C_f = I_8$.

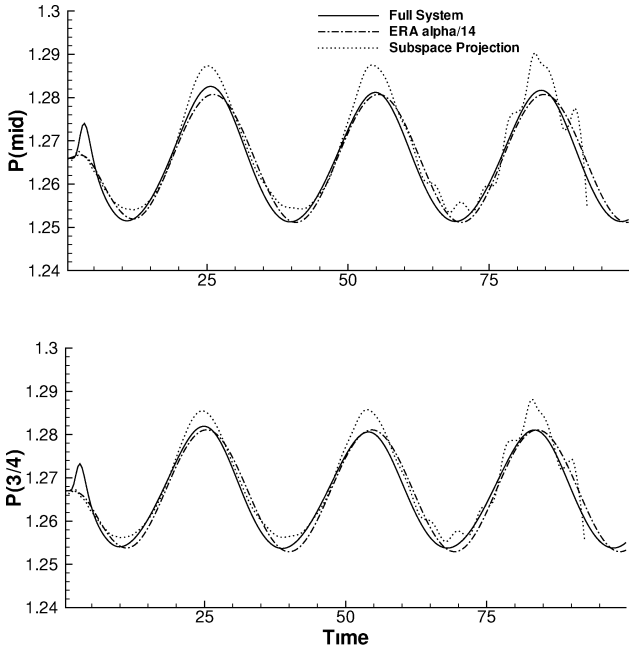

Fig. 5 Pressure time history on bump.

The impulse response of Eq. (28) was obtained with $\beta = 1$. Good agreement between the impulse response of the reduced-order system and the impulse response from the full-order system is shown in Fig. 3.

ROM Time Integration

In previous Volterra work, the choice of impulse amplitude and duration has been shown to have a strong affect on the accuracy of the reduced-order model.[30] Presently, no general rule is available to govern the choice of impulse amplitude. For this research, the impulse amplitude was arbitrary, and the scalar coefficient β introduced in Eq. (28) was used to synchronize the ROM results to match the full-order behavior. The full-order time history used to collect snapshot data for the POD development was available to set β; therefore, no additional full-order runs were required. The value of $\beta = 1/14$ was used to produce the results given next.

Modal Coefficients

The reduced-order fluid system [Eq. (28)] was time integrated with the baseline forcing, and the modal reponses were obtained as shown in Fig. 4. Good agreement with full-system modal amplitudes was shown for the same time-integration case. Full-system modal amplitudes were obtained by projecting the full-order response onto the modes.

Surface Pressure

In addition, the pressure on the surface of the bump was obtained from the reduced-order model by expanding the modal responses and extracting the pressures from the proper spatial locations. Surface pressures (at the midpoint and $\frac{3}{4}$-chord) from the POD-Volterra reduced-order model were shown to be in good agreement with the full-order results in Fig. 5 ($< 5\%$ average error). The same mode set was used in a subspace projection POD/ROM, and the results were not as accurate (also shown in Fig. 5). The subspace projection POD/ROM began to go unstable after the second cycle. We attempted to improve the subspace projection results by truncating more modes, but the solution accuracy suffered. The state-space approach with POD-Volterra stabilizes the high-frequency content in the lower energy modes, providing better accuracy than subspace projection for this case.

Quantifying Dissipation

The eigenvalues of the reduced-order system are shown in Fig. 6. For this plot, the discrete system from Eq. (28) is converted to

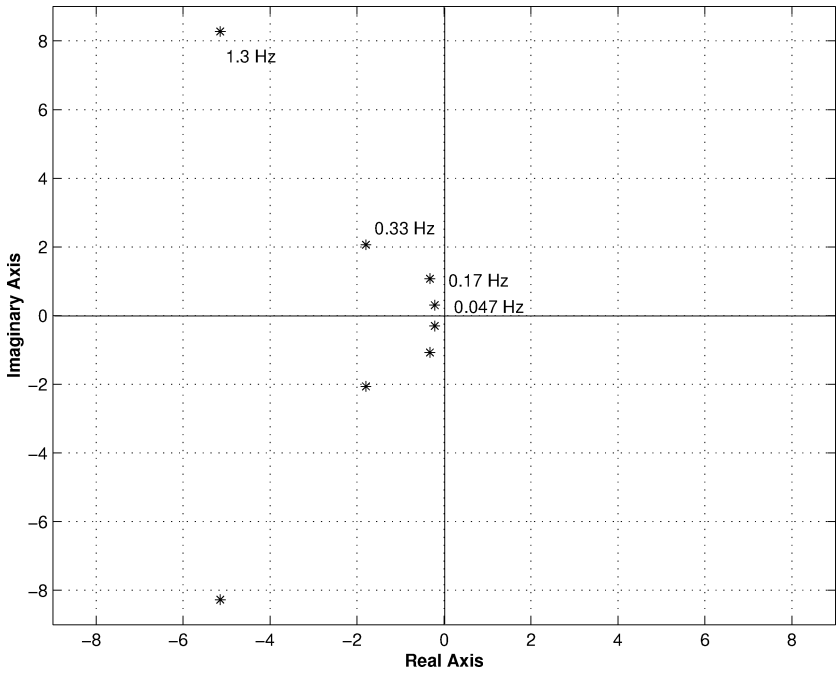

Fig. 6 Eigenvalues of ROM fluid system.

Table 1 Computational performance

Flow solver	DOFs	Wall-clock time, s
Full order	64,400	310.256
Subspace	8	77.902
POD-Volterra	8	0.08

continuous form, and the eigenvalues are obtained from the continuous version of A_f. The imaginary portion of each complex eigenvalue pair (jw) provides the frequency associated with that eigenmode. The baseline forcing frequency ($\omega = 0.2145$ radians per time unit) translates to 0.034 cycles per time unit (hertz). The frequency response of the full system in Fig. 2 is band limited, with the frequency response decaying rapidly after about 0.32 Hz. Clearly, the highest frequency (1.3 Hz) associated with the outlying eigenvalues in Fig. 6 represents nonphysical behavior, which is most likely caused by numerical instabilities in the full-system solver, transferred to the state-space model through the impulse response data. The second highest frequency (0.33 Hz) is close to the resonance peak and can represent legitimate physics in the system. The large, negative real portion of both high-frequency complex pairs represents the damping of the high-frequency oscillations. The large value of damping is consistent with the large amount of dissipation present at high frequencies in the first-order Roe-scheme fluid solver. The two low-frequency eigenvalues represent important physics in the modal amplitudes, and there is less damping of these terms in the state-space model.

Computational Performance

The motivation for employing the POD-Volterra approach was to realize a computational performance improvement consistent with the reduction in the number of DOFs. Computational performance, summarized in Table 1, was assessed by measuring the wall-clock time for each solver to provide a time history of the flow (88 time units). All computations were run on a 800-MHz Pentium-based PC. Both the full-system and non-Galerkin ROM solvers were written in FORTRAN by a single programmer. The compiler options and I/O requirements were chosen to provide the quickest run times, and these were identical for both the full-system and reduced-order solvers. The linear, state-space POD-Volterra ROM was time integrated on the same 800-MHz PC using a function call in MATLAB®.

The non-Galerkin approach was not nearly as efficient as the POD-Volterra method because the subspace projection method used the flux evaluation of the full-order model. Subspace projection mapped the flow solution onto the POD basis vectors at each integration step. This projection truncated high-frequency oscillations and permitted stable integrations at a Courant–Friedrichs–Lewy (CFL) condition of 5. (The full-order model required CFL < 1 for stability.) The larger time step associated with the large CFL number yielded the reduction in wall-clock time shown in Table 1. Notice that subspace projection only provided one-order-of-magnitude reduction in computation time to accompany four-order-of-magnitude reduction in DOFs. In contrast, the POD-Volterra ROM reduced compute time by four orders of magnitude and realized an improvement in performance consistent with the DOF reduction.

The cost of computing the state-space realization using ERA was small. Because there was one forcing term, only one additional run of the full order solver was required to provide the impulse response data. A single run of the full-order solver generally took about 300 s.

Conclusions

A new approach for generating reduced-order modeling (ROMs) of fluid systems was developed using proper orthogonal decomposition (POD) in combination with Volterra theory. The method involves identifying fluid basis functions with POD and applying systems realization theory to generate a linear, state-space model for the scalar coefficients. The method was tested on a two-dimensional inviscid flow over a bump with forcing. Eight POD basis functions were identified, and the eigensystem realization algorithm was used to identify an eight-state POD-Volterra ROM. Time histories of both the reduced-order coefficients and the flowfield data accurately tracked the full-order results in both amplitude and phase (average error less than 5%). The new approach was shown to be superior in accuracy, stability, and computational efficiency to the subspace projection POD/ROM for the same case. The POD-Volterra ROM demonstrated four-orders-of-magnitude reduction in compute time relative to the full system, which represents a computational improvement on the same order as the reduction in degrees of freedom.

The future of the hybrid POD-Volterra approach depends on extending the method to problems with moving boundaries and nonlinear dynamics. The extension to moving boundaries would require coupling the fluid model with a model of the boundary dynamics. Modal representation of the boundary would result in forcing terms for the system realization of the fluid dynamics, replacing the γ forcing used here. The impulse response from each boundary mode could be obtained from the full-system model, and these would comprise the Markov parameter for system realization. In the event of a free boundary, the fluid modes could also be used to force the boundary dynamics. In this manner, dynamic boundary conditions could be incorporated through the coupling of forcing terms.

The addition of nonlinear terms to the POD-Volterra ROM could come from two areas of research. Nonlinear-systems realization with Volterra theory is an active area of research[30] that is attempting to identify nonlinear state-space models from sampled data. For weakly nonlinear systems, a Galerkin approach to the Euler equations, along with of-order analysis to reduce the number of terms, might be a viable approach. Galekrin projection to identify the nonlinear terms could be used to amend the linear state-space model with the necessary nonlinear terms for specific problems.

The linear POD-Volterra ROM coupled with a nonlinear structural model could be used to study many aeroelastic problems of interest in an efficient and accurate manner. Many limit-cycle oscillation and flutter problems involve linear fluid dynamics and nonlinear structural dynamics. Elastic panels in supersonic crossflow are just one example. The tremendous computational speed associated with this new approach, combined with the potential for application to aeroelastic design problems, makes this hybrid approach an important advance in reduced-order modeling methods.

Acknowledgments

The authors gratefully acknowledge the U.S. Air Force Office of Scientific Research (Dean Mook) for supporting this work through Grant 99VA01COR. The views expressed in this paper are those of the authors and do not reflect the official policy or position of the United States Air Force, the Department of Defense, or the U.S. Government.

References

[1]Ito, K., and Ravindran, S. S., "A Reduced-Order Method for Simulation and Control of Fluid Flows," *Journal of Computational Physics*, Vol. 143, 1998, pp. 403–425.

[2]Shvartsman, S. Y., and Kevrekidis, I. G., "Nonlinear Model Reduction for Control of Distributed Systems: A Computer-Assisted Study," *American Institute of Chemical Engineering*, Vol. 44, No. 7, 1998, pp. 1579–1595.

[3]Banerjee, S., Cole, J. V., and Jensen, K. F., "Nonlinear Model Reduction Strategies for Rapid Thermal Processing Systems," *IEEE Transactions on Semiconductor Manufacturing*, Vol. 11, No. 2, 1998, pp. 266–275.

[4]Kunisch, K., and Volkwein, S., "Control of the Burgers Equation by a Reduced-Order Approach Using Proper Orthogonal Decomposition," *Journal of Optimization Theory and Applications*, Vol. 102, No. 2, 1999, pp. 345–371.

[5]Rediniotis, O. K., Ko, J., Yue, X., and Kurdila, A. J., "Synthetic Jets, Their Reduced Order Modeling and Applications to Flow Control," AIAA Paper 99-1000, Jan. 1999.

[6]Park, H. M., and Lee, M. W., "An Efficient Method of Solving the Navier–Stokes Equation for Flow Control," *International Journal for Numerical Methods in Engineering*, Vol. 41, 1998, pp. 1133–1151.

[7]Romanowski, M. C., and Dowell, E. H., "Reduced Order Euler Equations for Unsteady Aerodynamic Flows: Numerical Techniques," AIAA Paper 96-0528, Jan. 1996.

[8]Dowell, E. H., "Eigenmode Analysis in Unsteady Aerodynamics: Reduced-Order Analysis," *AIAA Journal*, Vol. 34, No. 8, 1996, pp. 1578–1583.

[9]Beran, P. S., Huttsell, L. J., Buxton, B. J., Noll, C., and Osswald, G., "Computational Aeroelastic Techniques for Viscous Flow," CEAS/AIAA/ICASE/NASA Langley International Forum on Aeroelasticity and Structural Dynamics, June 1999.

[10]Hall, K. C., Thomas, J. P., and Dowell, E. H., "Reduced-Order Modeling of Unsteady Small-Disturbance Flows Using a Frequency-Domain Proper Orthogonal Decomposition Technique," AIAA Paper 99-0655, Jan. 1999.

[11]Dowell, E. H., Hall, K. C., Thomas, J., Florea, R., Epureanu, B., and Heeg, J., "Reduced Order Models in Unsteady Aerodynamics," AIAA Paper 99-1261, April 1999.

[12]Florea, R., Hall, K. C., and Dowell, E. H., "Eigenmode Analysis and Reduced Order Modeling of Unsteady Transonic Full Potential Flow Around Isolated Airfoils," CEAS/AIAA/ICASE/NASA Langley International Forum on Aeroelasticity and Structural Dynamics, June 1999.

[13]Pettit, C. L., and Beran, P. S., "Reduced-Order Modeling for Flutter Prediction," *International Journal for Numerical Methods in Engineering*, Vol. 55, 2002, pp. 479–497.

[14]Mortara, S. A., Slater, J. C., and Beran, P. S., "An Optimal Proper Orthogonal Decomposition Technique for the Computation of Nonlinear Panel Flutter," AIAA Paper 2000-1936, April 2000.

[15]Beran, P., and Pettit, C., "Prediction of Nonlinear Panel Response Using Proper Orthogonal Decomposition," AIAA Paper 2001-1292, April 2001.

[16]LeGresley, P. A., and Alonso, J. J., "Airfoil Design Optimization Using Reduced Order Models Based on Proper Orthogonal Decomposition," AIAA Paper 2000-2545, June 2000.

[17]Dowell, E. H., and Hall, K. C., "Modeling of Fluid-Structures Interaction," *Annual Review of Fluid Mechanics*, Vol. 33, 2001, pp. 445–490.

[18]Epureanu, B. I., Hall, K. C., and Dowell, E. H., "Reduced Order Models of Unsteady Transonic Viscous Flows in Turbomachinery," *Journal of Fluids and Structures*, Vol. 18, No. 8, 2000, pp. 1215–1235.

[19]Epureanu, B. I., Hall, K. C., and Dowell, E. H., "Reduced Order Models in Turbomachinery Using Inviscid-Viscous Coupling," *Journal of Fluids and Structures*, Vol. 15, No. 2, 2001, pp. 255–276.

[20]Epureanu, B. I., Dowell, E. H., and Hall, K. C., "A Parametric Analysis of Reduced Order Models of Potential Flows in Turbomachinery Using Proper Orthogonal Decomposition," American Society of Mechanical Engineers Turbo-Expo 2001, Paper 2001-GT-0434, June 2001.

[21]Lucia, D. J., King, P. I., and Beran, P. S., "Domain Decomposition for Reduced-Order Modeling of a Flow with Moving Shocks," *AIAA Journal*, Vol. 40, No. 11, 2002, pp. 2360–2362.

[22]Lucia, D. J., Beran, P. S., and King, P. I., "Reduced Order Modeling of an Elastic Panel in Transonic Flow," *Journal of Aircraft*, Vol. 40, No. 2, 2003, pp. 338–347.

[23]Lucia, D. J., Beran, P. S., and Silva, W. A., "Reduced-Order Modeling: New Approaches for Computational Physics," *Progress in Aerospace Sciences*, Vol. 40, 2004, pp. 51–117.

[24]Lucia, D. J., King, P. I., and Beran, P. S., "Reduced Order Modeling of a Two Dimensional Flow with Moving Shocks," *Computers and Fluids*, Vol. 32, 2003, pp. 917–938.

[25]Silva, W. A., "Application of Nonlinear Systems Theory to Transonic Unsteady Aerodynamic Responses," *Journal of Aircraft*, Vol. 30, No. 5, 1993, pp. 660–668.

[26]Rugh, W. J., *Nonlinear Systems Thoery, The Volterra-Weiner Approach*, Johns Hopkins Univ. Press, Baltimore MD, 1981.

[27]Clancy, S. J., and Rugh, W. J., "A Note on the Identification of Discrete-Time Polynomial Systems," *IEEE Transactions on Automatic Control*, Vol. AC-24, No. 6 , 1979.

[28]Schetzen, M., "Measurement of Kernels of a Nonlinear System of Finite Order," *International Journal of Control*, Vol. 1, No. 3, 1965, pp. 251–263.

[29]Boyd, S., Tang, Y. S., and Chua, L. A., "Measuring Volterra Kernels," *IEEE Transactions on Circuits and Systems*, Vol. CAS-30, No. 8, 1983.

[30]Silva, W. A., and Bartels, R. E., "Development of Reduced Order Models for Aeroelastic Analysis and Flutter Prediction Using the CFL3Dv6.0 Code," AIAA Paper 2002-1594, April 2002.

[31]Tannehill, J. C., Anderson, D. A., and Pletcher, R. H., *Computational Fluid Mechanics and Heat Transfer*, Hemishpere, Washington, DC, 1997, pp. 321–367, 388–398.

[32]Stakgold, I., *Green's Functions and Boundary Value Problems*, 2nd ed., Wiley, Washington, DC, 1998, pp. 496, 498.

[33]Holmes, P., Lumley, J., and Berkooz, G., *Turbulence, Coherent Structures, Dynamical Systems and Symmetry*, Cambridge Univ. Press, Cambridge, England, U.K., 1996, pp. 86–108.

[34]Sirovich, L., "Turbulence and the Dynamics of Coherent Structures. Part 1: Coherent Structures," *Quarterly of Applied Mathematics*, Vol. 45, No. 3, 1987, pp. 561–571.

[35]Naylor, A. W., and Sell, G. R., *Linear Operator Theory in Engineering and Science*, Springer-Verlag, New York, 1982, pp. 161–165.

[36]Lucia, D. J., "Reduced Order Modeling for High Speed Flows with Moving Shocks," Ph.D. Dissertation, School of Engineering and Management, Air Force Inst. of Technology, Dayton, OH, Nov. 2001.

[37]Silva, W. A., "Discrete-Time Linear and Nonlinear Aerodynamic Impulse Responses for Efficient CFD Analyses," Ph.D. Dissertation, College of William and Mary, Williamsburg, VA, Dec. 1997.

[38]Silva, W. A., "Reduced-Order Models Based on Linear and Nonlinear Aerodynamic Impulse Responses," *CEAS/AIAA/ICASE/NASA Langley International Forum on Aeroelasticity and Structural Dynamics*, 1999, pp. 369–379.

[39]Raveh, D., Levy, Y., and Karpel, M., "Aircraft Aeroelastic Analysis and Design Using CFD-Based Unsteady Loads," AIAA Paper 2000-1325, April 2000.

[40]Volterra, V., *Theory of Functionals and of Integral and Integro-Differential Equations*, Dover, New York, 1959.

[41]Schetzen, M., *The Volterra and Wiener Theories of Nonlinear Systems*, Wiley, New York, 1980.

[42]Bendat, J. S., *Nonlinear System Analysis and Identification from Random Data*, Wiley-Interscience, New York, 1990.

[43]Juang, J. N., and Pappa, R. S., "An Eigensystem Realization Algorithm for Modal Parameter Identification and Model Reduction," *Journal of Guidance, Control, and Dynamics*, Vol. 8, No. 5, 1984, pp. 620–627.

[44]Beran, P. S., Lucia, D. J., and Pettit, C. L., "Reduced Order Modeling of Limit-Cycle Oscillation for Aeroelastic Systems," American Society of Mechanical Engineers, IMECE 2002-32954, Nov. 2002.

[45]Sankar, L. N., Ruo, S. Y., and Malone, J. B., "Application of Surface Transpiration in Computational Aerodynamics," AIAA Paper 86-0511, Jan. 1986.

[46]Kaplan, C., "The Flow of a Compressible Fluid Past a Curved Surface," NACA Rept. 768, 1944.

K. N. Ghia
Associate Editor